An evaluation of meteorological data prediction over Washington, D.C.: Comparison of DCNet observations and NAM model outputs

Nebila Lichiheb*[1], Bruce Hicks[2], LaToya Myles[1]

[1]*National Oceanic and Atmospheric Administration (NOAA), Air Resources Laboratory, Oak Ridge, TN 37831-2456, USA.*

[2]*MetCorps, PO Box 1510, Norris, TN 37828, USA.*

Corresponding author*: Nebila Lichiheb

Email: nebila.lichiheb@noaa.gov

Abstract

This study presents an example of how outputs of operational and readily-available mesoscale numerical models can be adapted to initialize dispersion calculations within the urban surface roughness layer. Three years of urban meteorological observations from central Washington, DC, are compared against forecast outputs of the North American Mesoscale (NAM) model. NAM wind speed predictions underestimate the observations in light winds and overestimate the measurements in high winds. Average wind directions are consistent. However, an adjustment of the predicted direction of the plume by -20° is needed. The uncertainty associated with this adjustment is large in light NAM wind speed with no evident variation by season. The values of the standard deviation of the wind direction, σ_θ derived from NAM model outputs underestimate the observations by a small amount (about -1.5 to -2.5 degrees). The results presented here indicate that mesoscale numerical model outputs can provide information adequate for dispersion calculations. However, levels of uncertainty associated with implementation of the suggested procedures increase with decreasing wind speed, causing considerable uncertainty in the implementation of adjustments as low wind speed conditions are approached. Results and recommendations reported here should not be extended to other numerical models or other cities without further testing.

Key words: Dispersion, NAM model, DCNet observations, Washington, D.C.

1. Introduction

Currently, more than 50% of the world's population lives in urban areas. That percentage is expected to grow to about 70% by 2050 (United Nations, 2019). The United States is one of the most urbanized regions in the world with 80% of the population living in urban areas (Leeson, 2018). This trend in urbanization has led to a significant impact on local weather and atmospheric structure in various ways. The most thoroughly investigated aspect of urban climate modification is the urban heat island (Oke, 1987; Arnfield, 2003). The urban heat island refers to the atmospheric warmth of a city and its effects on its surroundings; it occurs in and extends downwind from all urban areas in warm or cold climates (Stewart and Oke, 2012). Other scientific studies have shown that urbanization can alter the hydrological system by creating an increase in regional precipitation variability and intensity (Yang et al., 2013; Hand and Shepherd, 2009; Shepherd, 2006). Air quality and urban pollution are other major issues related to the increase of the urban population. The considerable increase in industrialization and traffic have been associated with elevated hazardous material releases and greenhouse gas emissions (Kelly and Fussell, 2015; Pataki et al., 2007). Atmospheric dispersion and deposition of hazardous materials in urban areas are therefore increasingly under investigation due to the potential impact on human health and the environment.

The expected growth of urban populations imposes an expanded need for more accurate prediction of urban meteorology, and especially of the risk following release of some hazardous material into the air. Assessments of the adverse effects of pollutants in urban areas require detailed description of the atmospheric wind fields affecting them. Researchers usually prefer to rely on predictions made using the most advanced simulation available, often tuned to optimize the ability to relate to the specific area of interest. In practice, responders to an event involving a release of some hazardous material will have little opportunity to select the meteorological simulation most suited to the site-specific circumstances involved. Instead, reliance is typically on forecast models routinely vetted and familiar to the emergency response community, including several models from the National Oceanic and Atmospheric Administration (NOAA) National Weather Service (NWS). Within the United States, the products of these models are available for use as inputs to several operational dispersion models (Seaman, 2000).

Due to the complexity of urban land surfaces, meteorological models for the urban environment are still under development, even in a research setting (Baklanov et al., 2018). One concept of further model research and development is "skimming flow" which refers to the decoupling of the atmospheric flow within street canyons from the flow entering the urban environment above the rooftops, due to the presence of buildings, streets, vegetation, etc. (Britter and Hanna, 2003). Changes in surface roughness by street canyons and buildings cause an increase in turbulent mixing and a slowing of the local flow within the urban core (Roth, 2000; Kanda, 2007). Due to the complexity of the urban areas, operational weather prediction models may have large biases in urban environments. In general, NWS models have very limited information about the underlying urban environment because they do not include the urban topography to address the increased turbulence imposed by the different obstacles. Therefore, an additional surface roughness is applied to describe the slowing of the local flow as well as the increasing of the turbulent mixing level, known as the roughness approach (Martilli, 2002). This empirical adjustment only addresses the overall flow structure by assuming stationary conditions and spatial homogeneity. To address this issue, urban canopy parameterizations have been developed and implemented in fine grid spacing meteorological models (Otte et al., 2004), however this parameterization includes lots of uncertainties. Furthermore, such forecasting models are not based on observations within the urban core but on micrometeorological data typically gathered tens of kilometers away in less densely populated settings. Contributing micrometeorological stations are usually located at a major airport where conditions are considerably different from downtown (Hicks, 2005).

To improve urban atmospheric dispersion simulations, an initial priority of this work is to provide more accurate wind field descriptions. Seldom are local wind observations available in urban areas, and if they exist, they are typically not ingested into routinely available numerical weather models. In this context, Haupt et al. (2019) highlighted the need to combine observations and NWS model simulations to provide a more accurate meteorological inputs to operational air pollution models. Local observations provide opportunities to test the relevance of model predictions and to quantify the relevant uncertainty. This uncertainty information is needed for both dispersion assessment and practical emergency response (Dabberdt et al., 2000).

To address some of these uncertainties, a research program (DCNet) was established in 2003 by the NOAA Air Resources Laboratory (ARL) to collect micrometeorological information at multiple sites across the Washington, DC, area, with the dual intent (a) to provide a basis for examining and refining the relevance of meteorological information provided by routine weather forecasting sources, and (b) to provide on-site wind field data on which to base dispersion models for emergency application. Hicks et al., (2012) reviewed data obtained from DCNet and showed the utility of such data for evaluating the relevance of guidance from NWS models and improve the description of atmospheric dispersion in urban areas. The extended DCNet data record is unique and provides an opportunity to resolve some of the complexities of the urban environment.

The main goals of this study are to demonstrate the differences arising when routine model outputs are compared with urban observations and to quantify the adjustments required when model outputs are used to represent the downtown business district of Washington, DC. The focus is on the comparison of wind observations from the DCNet station on the U.S. Department of Commerce Herbert C. Hoover Building (HCHB) and the North American Mesoscale (NAM) model outputs for the period 2017-2019. The NAM model has been chosen as an example of possible wind field guidance, unaffected by model adjustment to improve agreement with local conditions (as is a common issue arising when research-grade models are employed).

The analysis presented here uses existing data from the DCNet research network (Hicks, 2005; Pendergrass et al., 2020) as a basis for examining the relevance of wind field predictions by a large-scale synoptic simulation, such as the NAM model. In the first part of the analysis to follow, HCHB wind observations will be compared against NAM outputs using a seasonal regression analysis. In the second part, the average differences in wind speed and wind direction between NAM outputs and HCHB observations will be analyzed seasonally as a function of NAM wind speed and as a function of time of day. A third part will extend considerations to the quantification of the plume-spreading estimates, the standard deviations of the wind direction σ_θ. Methods for adjusting outputs from the NAM model to improve agreement with DCNet observations will be proposed.

2. Data selection and analysis

In terms of making best use of existing data to improve dispersion model predictions for urban and city applications, the DCNet data provide a unique opportunity for real-time meteorological observations over the greater National Capital Region (NCR) to support development of numerical weather prediction models as well as provide the meteorological observations to initialize for atmospheric transport and diffusion models (Hicks et al., 2012). The NCR was selected as the focal area because of: (i) its known status as a target for terrorist attack, (ii) its history as a site for research using atmospheric tracers (Draxler, 1987a, b; Draxler, 2006), and (iii) the unusually confined building dimensions (with building heights not exceeding about 27 m as required by the Washington Building Act of 1910). The data are therefore collected in an area with fairly uniform density and height of buildings. In conjunction with the relative simplicity of the terrain, Washington, D.C. is a testbed for such study, providing a case of skimming flow where the assumptions of horizontal homogeneity and stationarity are approximated more than in other cities (Hicks et al., 2014).

The locations of DCNet measurements are spread across the District of Columbia and its surrounding suburbs. Of these stations, the installation atop the U.S. Department of Commerce Herbert C. Hoover Building (HCHB) at 1401 Constitution Avenue, Northwest, Washington, DC (38.894^{0}N, 77.033^{0}W) has been the subject of most recent attention. The building height is approximately 25 m above street level and about 28 m above sea level. This location is within the Central Business District (CBD) of Washington, is within 1 km of the White House. This DCNet station served as the central point within the NCR and has been unaffected by data interruptions caused by resource limitations. The HCHB station was installed in 2003 with data archiving starting in 2004. All available data collected at HCHB for the period from 1 January 2017 to 12 December 2019 have been used here without imposing any data screening.

Measurements were made using a 10-m meteorological tower above the HCHB rooftop (Figure 1). The tower is equipped with a three-dimensional sonic anemometer system, installed on the top and providing 10 m wind observations at a frequency of 10 Hz. Therefore, wind measurements are taken at about 35 m above street level. As for all DCNet installations, the tower is situated to minimize possible effects of roof edges and local obstructions. Averages, variances and covariances are computed by on-site data recording systems. All recorded data are transmitted every 15 minutes to a central archive, using cellular modems. Once received, data are subjected to coordinate rotation and error checking analyses. More details on the description of instrumentation and data analysis associated with the HCHB are presented by Pendergrass et al. (2020).

Figure 1: DCNet tower at the HCHB station, showing a sonic anemometer at the top of the roof-mounted 10m tower. The meteorological tower also includes instruments to measure air temperature, relative humidity and net radiation at the same height as the sonic anemometer.

An immediate question arises as to the representativeness of the HCHB dataset. To examine this, sonic anemometer data derived during 2008 have been analyzed for 7 DCNet stations within the NCR. Figure 2 shows (in red) the stations considered, with the HCHB site being identified by the square symbol. The locations of other DCNet locations, not contributing to the present CBD focus, are also depicted.

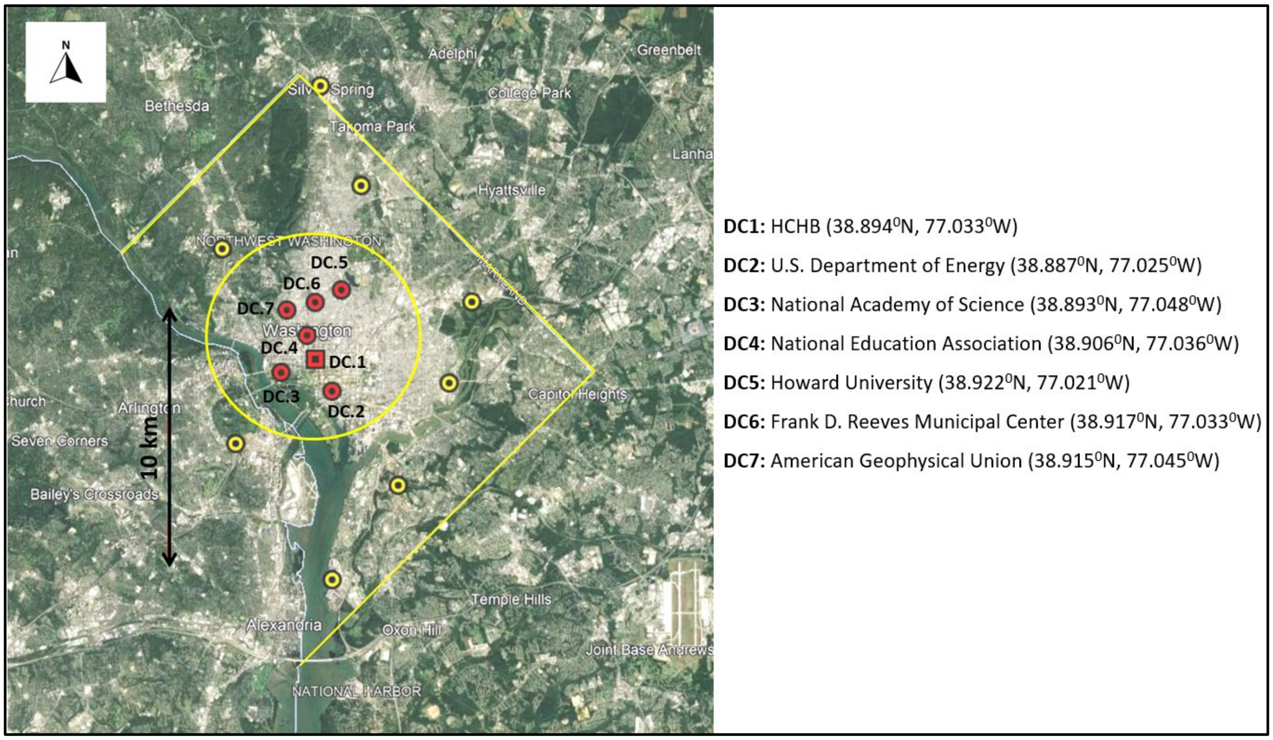

Figure 2: The DCNet locations (in red) used in an examination of the representativeness of individual stations, using 2008 data. The square identifies the Department of Commerce (HCHB) location. Yellow circles show DCNet locations excluded from the present analysis. Figure based on Google Earth.

Figure 3a shows the variation of wind speed with time derived for each of the red locations in Figure 2. Figure 3b shows the corresponding sequence for the standard deviation of wind direction. To illustrate the data variability, changes in the coefficient of variation (CV) are also plotted. (CV is the absolute value of the ratio of the standard deviation to the mean.) The comparison of the wind speed and standard deviation of wind direction data demonstrates the representativeness of the HCHB site measurements. The uniformity of the observations indicates rare departures from a coherent flow regime across the entire central DC area. Moreover, the low CV values in Figures 3a and 3b confirm that wind measurement from any DCNet location within the CBD can be considered to be representative of the area except for rare occasions when the CV approaches unity.

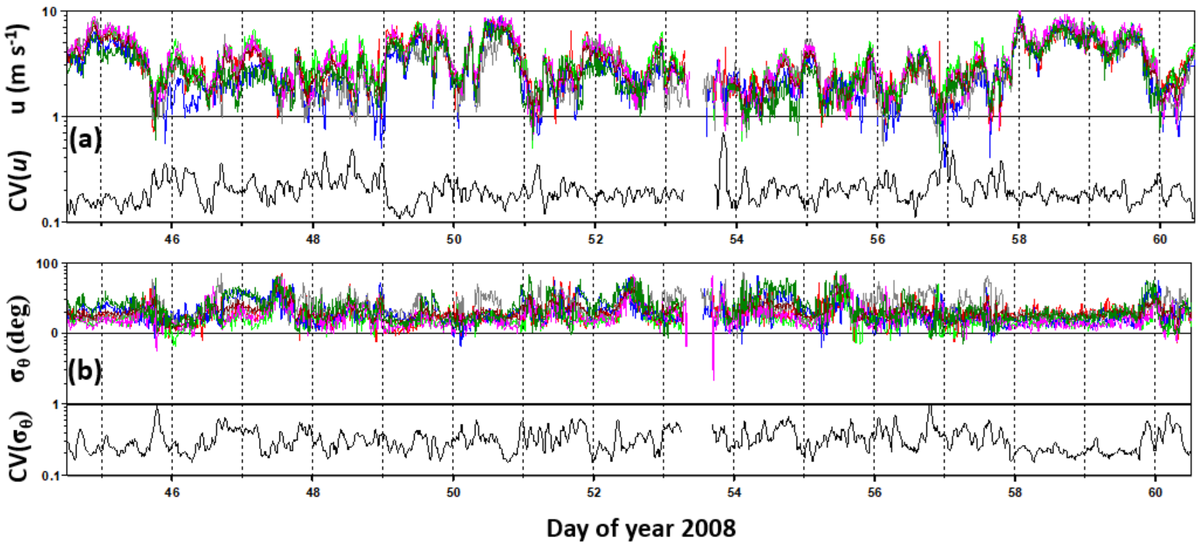

Figure 3: DCNet wind observations at 10 m height above rooftops from 7 stations (presented with 7 different colors) within the Washington, D.C. downtown area: (a) wind speed (u) and the changes in the Coefficient of Variation for wind speed (CV(u)), and (b) standard deviation of wind direction (σ_θ) and the changes in the Coefficient of Variation for wind direction (CV (σ_θ)). Coefficients of variation (CV) are plotted with black curves ($\mathrm{CV}(x) \equiv \sigma(x)/\bar{x}$).

The present study focuses on the relationship between velocity observations at the DOC (HCHB) DCNet location and routinely-provided predictions by the 12-km NAM model of NCEP. Following the same procedures that produced the measurements plotted in Figure 3, this analysis will make use of coordinate rotation to align with the mean wind direction and so that the average vertical wind speed $\overline{w}$ is zero (McMillen, 1988). The coordinate rotation yields an average wind speed "$\bar{u}_{\mathrm{HCHB}}$". Average wind directions "$\bar{\theta}_{\mathrm{HCHB}}$" are derived from the average $\overline{U}$ and $\overline{V}$ Cartesian velocity vectors reported by the sonic anemometry.

Predictions to be used in the comparisons to follow have been derived from the velocity simulations of the 12 km parent domain of the North American Mesoscale model (12 km NAM) (Black, 1994). The 12 km NAM is one of the forecast systems of the National Center for Environmental Predictions (NCEP). For a summary of these capabilities, see https://mag.ncep.noaa.gov/model-guidance-model-area.php. The NAM model provides predictions four times each day, at 0000, 0600, 1200, and 1800 UTC; it is initialized using a 6-h data assimilation cycle with hourly analysis updates using the NCEP hybrid variational ensemble analysis (q.v. NCAR, 2021). The NAM 12 model has been chosen in this study as an example. We assume that the HCHB rooftop represents the model surface. NAM provides geographic wind vectors at 10 m above the relevant zero-plane displacement, which are then assumed to be comparable to the 10 m wind observations above the rooftop at the HCHB site. NAM outputs have been used in this study without any adjustments of the land-surface characteristics. The 12 km grid size is considered to be optimal for this study because it is of similar scale to the study area; a smaller grid size would impose the need to account for topographic effects such as are known to be due to the Potomac River valley but are not appropriately detected by the DCNet array.

NAM provides quantifications of the wind vectors $\overline{U}$ and $\overline{V}$ hourly. From these hourly values, wind speed "$\bar{u}_{\mathrm{NAM}}$" and wind direction "$\bar{\theta}_{\mathrm{NAM}}$" were derived. NAM wind outputs relate to the final 15 min preceding every hour. These hourly "snapshot" wind estimates provided by NAM have then been compared to the last 15 min interval of the hour of data collection at the HCHB site.

3. Comparison of HCHB observations with NAM outputs

The comparison between wind speed and wind direction measurements from HCHB against the predictions of NAM has been focused on the error involved if modelers rely on NAM predictions alone. To this end, the differences in wind speed and wind directions, NAM – HCHB have been emphasized. Regarding wind direction, special attention has been directed to the issues arising when one of the measurements indicated east of north and the other west of north. The intent is to arrange for the most robust statistical examination possible, and hence the north-crossing issue has received considerable attention. In particular, when the difference $\bar{\theta}_{\mathrm{NAM}}$ - $\bar{\theta}_{\mathrm{HCHB}}$ in wind direction is more than 180°, 360° has been subtracted from it. In this way the range of wind direction departures is limited to $-180° < \bar{\theta}_{\mathrm{NAM}} - \bar{\theta}_{\mathrm{HCHB}} < 180°$.

Since the Washington D.C. area is well forested, differences in wind speed and wind direction between NAM and HCHB have been analyzed seasonally for the period from 1 January 2017 to 12 September 2019. The intent is to test whether the vegetative cover affects the dispersion input variables.

As a first step, HCHB velocity (speed and direction) measurements have been regressed against the NAM model outputs for each season, yielding the following relationships:

$$\bar{u}_{NAM} = a\,\bar{u}_{HCHB} + b \tag{1}$$

$$\bar{\theta}_{NAM} = a\,\bar{\theta}_{HCHB} + b \tag{2}$$

where a and b are the linear regression best fits for each variable and each season.

Table 1 summarizes the seasonal regression results. Seasons are defined in this study as January–March (winter), April–June (Spring), July–September (Summer), and October–December (Autumn). For wind speed, a and b values are consistent over the three years. However, the values of b are consistently less than unity, indicating the expected reduction of the wind speed (observed) from that predicted by the forecasting model. There is also a consistent offset involved, such that the regression line is displaced by about 0.5 m s^{-1}, with the observed wind speed always being lower than predicted.
and NAM simulations during the summer season may also be related to the consequences of greater summertime convection. This result is consistent with the findings of Pan et al., (2021) who investigated the seasonal variation of wind speed forecast errors of the WRF model over China and demonstrated that due to more active local convection during summer time, the urban velocity regime is difficult to simulate using Numerical Weather Prediction (NWP) models.

In the case of wind direction, the values of R^2 are higher than in the case of the wind speed. The roughness of the urban area affects the wind speed more than the wind direction. The values listed indicate that there is little reason to dispute the NAM wind direction predictions. The slopes of the regression lines (a) are all close to unity and their offsets (b) vary significantly although indicating consistent average offsets in the winters and autumns. *P*-values are also calculated for the seasonal regression of wind speed and wind direction for the years 2017–2019 (Table 1). The results show very small *p*-values ($p < 0.01$), indicating statistically significant linear regressions.
that the agreement between NAM and DCNet observations is most robust in the winter and least robust in the summer, with the other seasons being between these extremes. One interpretation of these observations is that thermal mechanisms (as in summer and winter, when building heat controls are major contributors to local heat balances, q.v. Hicks et al., 2010) are significant contributors. However, the present data are not adequate to reveal whether an explanation lies in the urban heat island effect or to the synoptic meteorological patterns which may change the

surface-energy budget and the thermal structure (Britter and Hanna, 2003). Furthermore, our results do not show a significant impact of the vegetation cover on wind observations.

Table 1: Summary of the seasonal regression analysis results for wind speed and wind direction for the years 2017–2019. R^2 is the coefficient of determination, a is the slope and b is the offset, assuming a linear dependence of the kind $\bar{u}_{\mathrm{NAM}} = \mathrm{a}\ \bar{u}_{\mathrm{HCHB}} + \mathrm{b}$ and $\bar{\theta}_{\mathrm{NAM}} = \mathrm{a}\ \bar{\theta}_{\mathrm{HCHB}} + \mathrm{b}$, with $\bar{u}_{\mathrm{NAM}}$, $\bar{u}_{\mathrm{HCHB}}$, $\bar{\theta}_{\mathrm{NAM}}$, and $\bar{\theta}_{\mathrm{HCHB}}$ refer to NAM wind speed, HCHB wind speed, NAM wind direction, and HCHB wind direction respectively. *P*-value is the level of significance of the linear dependence.

		Wind speed (m/s)				Wind direction (deg)			
		R2	a	b	*p*-value	R2	a	b	*p*-value
2017	Winter	0.67	0.92	0.34	9.86 E-03	0.85	1.00	-20.45	2.27 E-107
	Spring	0.62	0.90	0.70	9.96 E-66	0.82	0.92	0.30	4.20 E-62
	Summer	0.49	0.78	0.73	5.82 E-20	0.80	0.92	-4.34	2.61 E-71
	Autumn	0.69	0.99	0.43	4.07 E-42	0.87	1.00	-18.07	7.15 E-51
2018	Winter	0.64	0.93	0.55	5.41 E-24	0.92	1.02	-20.68	6.43 E-103
	Spring	0.56	0.83	0.76	3.92 E-26	0.77	0.91	-1.19	6.35 E-58
	Summer	0.49	0.80	0.75	5.27 E-31	0.80	0.92	-10.73	4.20 E-111
	Autumn	0.64	0.91	0.53	1.11 E-27	0.87	0.99	-14.79	4.99 E-85
2019	Winter	0.68	0.99	0.22	1.11 E-13	0.90	1.01	-19.80	5.67 E-93
	Spring	0.61	0.92	0.74	9.66 E-91	0.83	0.93	-2.51	1.59 E-68
	Summer	0.41	0.68	0.98	2.12 E-16	0.72	0.89	1.78	3.88 E-52

Figure 4 shows an example for the spring season of 2017, showing the scatter affecting an over-riding linear relationship.

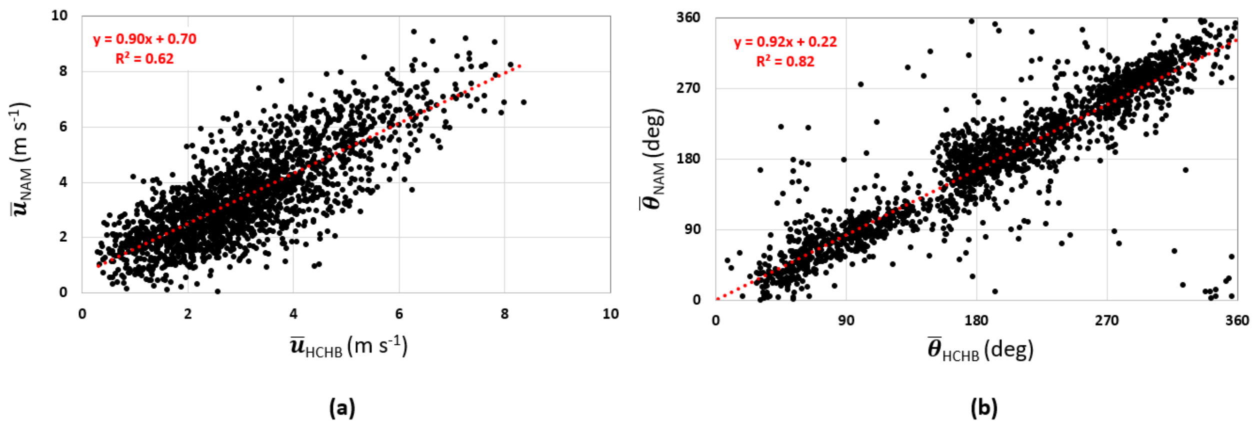

Figure 4: Linear regressions of $\bar{u}_{\mathrm{NAM}}$ against $\bar{u}_{\mathrm{HCHB}}$ (a) and $\bar{\theta}_{\mathrm{NAM}}$ against $\bar{\theta}_{\mathrm{HCHB}}$ (b) for the spring season of 2017.

4. Deriving wind adjustments

In examining differences between predictions of a selected routine weather forecast model and on-site observations, the focus of the considerations to follow is on the basic requirements for emergency-response dispersion modeling: the average wind speed and direction ($\bar{u}$ and $\bar{\theta}$ respectively) and the familiar dispersion spread quantity σ_θ. (As is common in meteorology, overbars are used to represent time averages). In all three cases, the analysis will address both the magnitudes of the differences between predictions and observations and the uncertainties associated with these differences. To avoid confusion arising from consideration of standard deviations among sets of measurements of $\bar{\theta}$ when the dispersion variable σ_θ is a more familiar quantity, the uncertainty associated with differences (predictions minus observed) of all average quantities will be identified using the symbol ξ, so that $\xi(\bar{u})$ is the root mean square departure of the differences between predictions of $\bar{u}$ and observations.

Inspection of the data on which the regressions of Table 1 were based shows that the wind direction correspondence, HCHB to NAM, decreased rapidly as wind speed dropped, such that the values of b and hence of $\xi(\bar{\theta})$ are greatly affected by the large differences encountered when conditions are near calm. To address this issue, more detailed analyses of the available data have proved useful, as will follow.

4.1. Wind speed

In order to quantify the NAM wind speed error, the difference in velocity between NAM outputs and HCHB observations has been scrutinized more thoroughly. Available data within each season were ordered by $\bar{u}_{\mathrm{NAM}}$ and grouped into sequential hundred data points. For each sequence, averages of the differences $\delta\bar{u} = (\bar{u}_{\mathrm{NAM}} - \bar{u}_{\mathrm{HCHB}})$ were obtained, together with quantification of the standard deviation of the departure of average wind speeds $\xi(\delta\bar{u})$. Very small p-values ($p \sim 0$) were obtained for the different regressions presented in Figure 5, indicating statistically significant linear regressions. Results are shown in Figure 5, where it is seen that for NAM derived wind speeds between 2 and 5 m s^{-1}, NAM and HCHB generally agree quite well. However, NAM significantly underestimates the observations at low wind speeds (< 2 m s^{-1}) and significantly overestimates the measurements at high wind speeds (> 5 m s^{-1}). As illustrated by the linear regression lines, there is no significant difference between the seasons and the results are similar for the years 2017, 2018 and 2019. Based on the average linear regression, the HCHB wind speeds should be estimated from the NAM model outputs as follows:

$$\bar{u}_{(adjusted)} = 0.66\, \bar{u}_{NAM} + 0.81 \tag{3}$$

This result is consistent with other studies that have shown that for urban and city applications NWP models do not perform well for very low and high wind conditions (Ngan et al., 2015; Pan et al., 2021; Samalot et al., 2019). The wind biases depend on the magnitude of wind speed for all seasons.

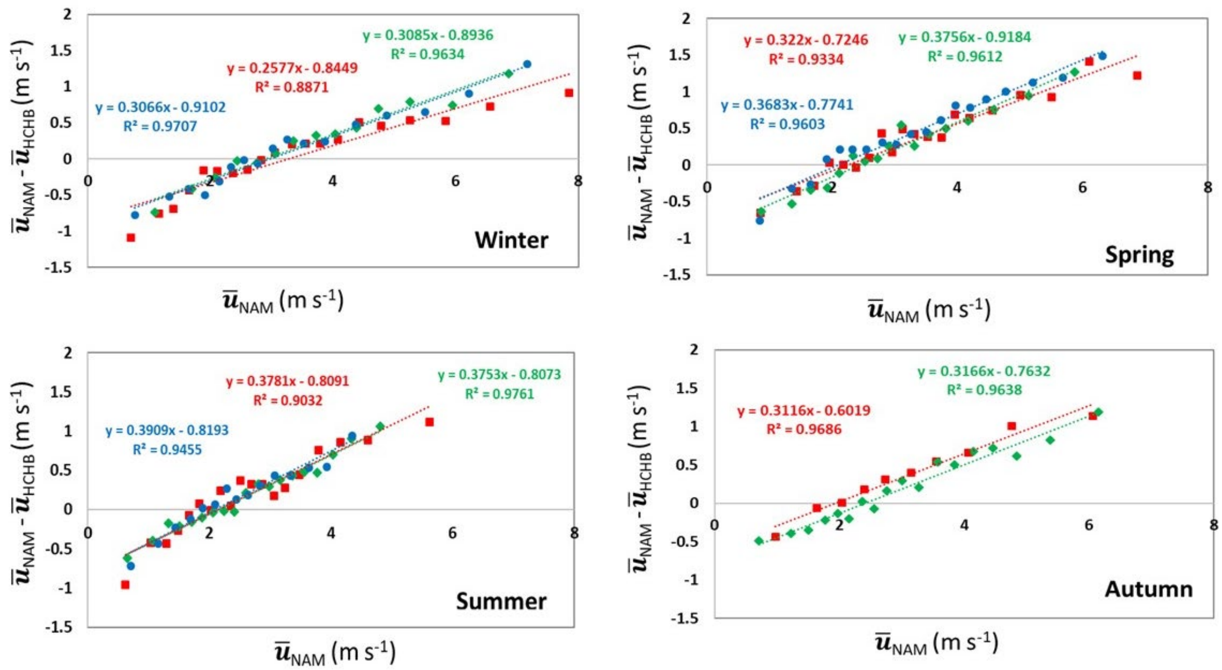

Figure 5: Regression analyses of the difference in average wind speed between NAM outputs and HCHB observations against NAM wind speed for the years 2017–2019. Red squares, green diamonds, and blue circles indicate the years 2017, 2018 and 2019, respectively. *P*-values of the different regressions for the years 2017, 2018 and 2019 are almost equal to zero ($p \sim 0$). For presentation clarity, every hundredth data point is displayed.

The data available here gives the error margin that a modeler needs to consider by implementing the proposed adjustment in equation 3. Figure 6 shows results derived when the uncertainties of the differences between NAM output wind speeds and HCHB observations ($\xi(\delta\overline{u})$) are plotted against NAM wind speed. Very small *p*-values ($p \sim 0$) were also obtained here (Figure 6), indicating statistically significant correlations. The plots of Figure 6 reveal similarity among the results from the different seasons and different years. The average of the results shown in Figure 6 permit a direct quantification of the uncertainties associated with such an adjustment.

$$\xi\,(\overline{u}_{(adjusted)}) = 0.07\,\overline{u}_{NAM} + 0.63 \qquad (4)$$

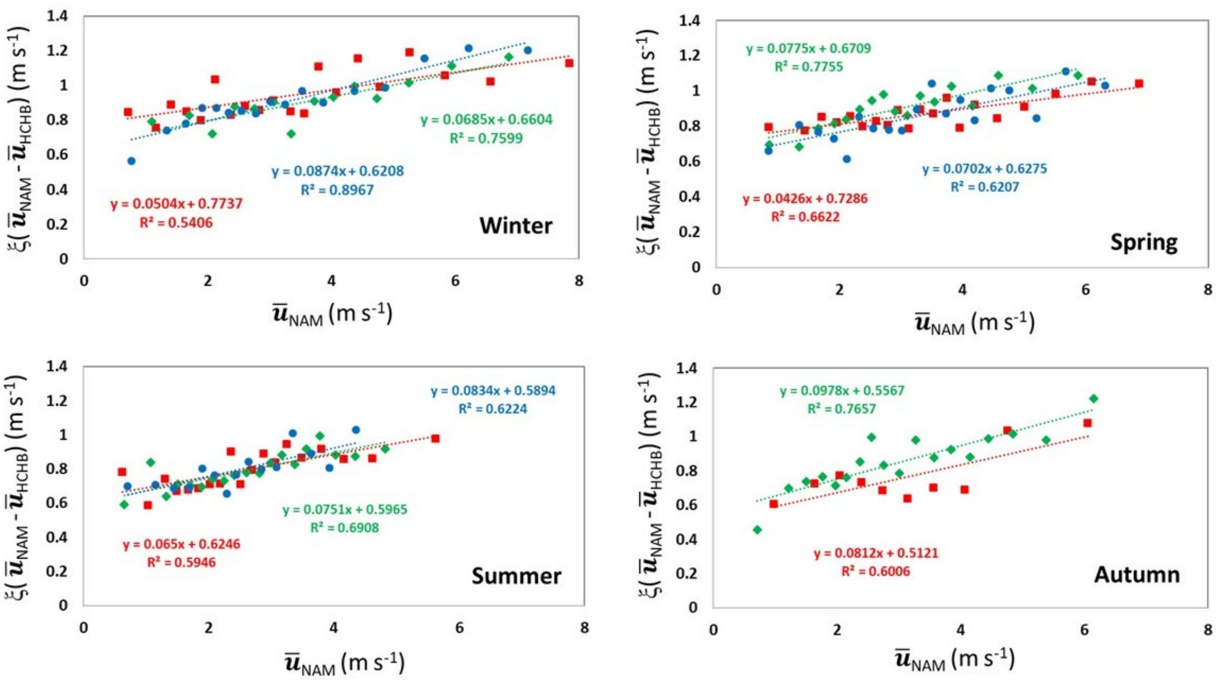

Figure 6: Analyses of the standard deviations of the difference in wind speed between NAM outputs and HCHB observations against NAM wind speed for the years 2017–2019. Red squares, green diamonds, and blue circles indicate the years 2017, 2018 and 2019, respectively. *P*-values of the different regressions for the years 2017, 2018 and 2019 are almost equal to zero ($p \sim 0$). For presentation clarity, every hundredth data point is displayed.

In practical application of the wind speed results reported here, it is anticipated that a modeler will (a) compute the wind speed ($\bar{u}_{NAM}$) from the vector outputs ($\bar{U}$ and $\bar{V}$) of the forecast model (NAM in the present case), (b) use Eq. 3 to estimate the wind speed appropriate for the NCR, and then use Eq. 4 to compute the uncertainty associated with the revised wind speed quantification. Basing this last step on Eq. 4 results in an identification of the root mean square error in the adjustment (the relevant standard deviation), which is now shown to be a slowly changing function of the wind speed. Thus, the relevant average wind speed is derived, along with the uncertainty associated with it.

4.2. Wind Direction

The summary of wind direction correspondence between NAM products and HCHB observations presented in Table 1 indicates substantial variability in the results of a simple linear regression approach. The matter requires additional attention, as in Figure 7. The uppermost panels of Figure 7 show how the difference in average wind direction between NAM outputs and HCHB observations varies as a function of NAM wind speed. The lower panels show the variation of the same differences with time of day. Error bars correspond to ± one standard deviation. These examples are for the summer 2017, spring 2018 and winter 2019. The illustrations indicate that there is a consistent difference between average NAM predictions of wind direction and 15 min average HCHB observations, regardless of whether changes are quantified according to $\bar{u}_{\mathrm{NAM}}$ or time of day. The consistent difference appears to be about - 20 deg (one standard deviation). However, the uncertainty associated with this difference decreases with increasing $\bar{u}_{\mathrm{NAM}}$, but not according to the time of day.

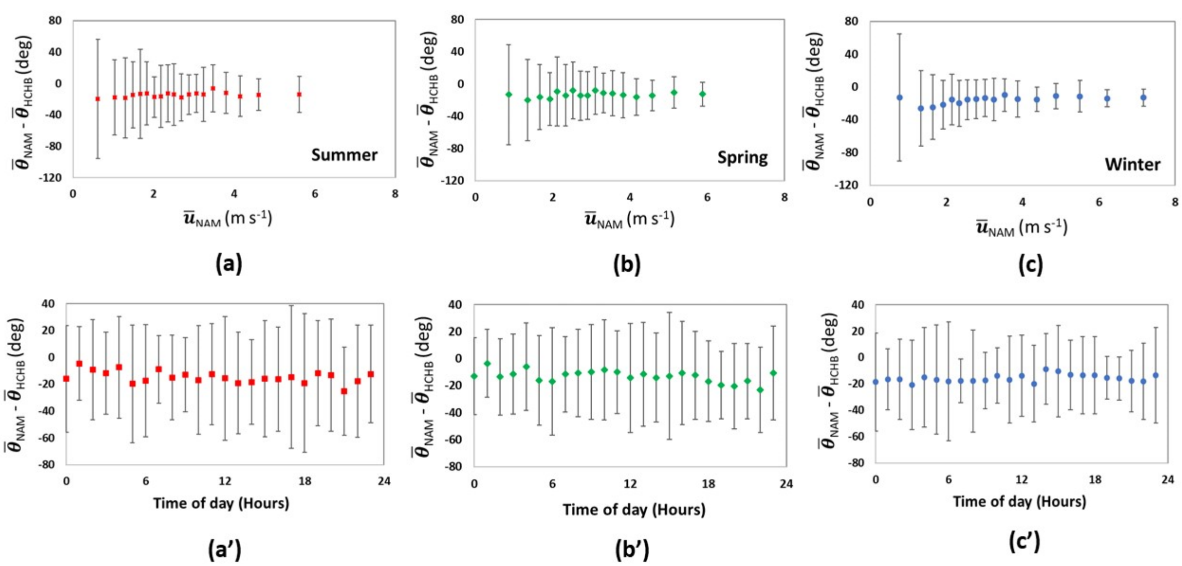

Figure 7: In the uppermost panels, results derived from the average differences in wind direction between NAM outputs and HCHB observations against NAM wind speed during the summer 2017 (a), spring 2018 (b) and winter 2019 (c). In the lower three panels, the same differences expressed as a function of time of day. Error bars represent ± one standard deviation.

Following the procedure used above to examine the extrapolation of wind speed from NAM predictions, the uncertainties of the differences in wind direction between NAM average velocity outputs and HCHB observations (ξ(δ is plotted as a function of NAM wind speed in Figure 8. The result reveals a strong dependence of the wind direction departure on NAM wind speed for the entire study period with no detectable variation by season. Note that the error appears to asymptote about 15 deg as wind speed increases, this quantifying the accuracy that cannot be improved. Inspection of the data reveals that the dependence is according to the inverse of the wind speed. Accordingly, the ordinate values corresponding to the plot of Figure 8 have been regressed against $1/\bar{u}_{NAM}$, and the resulting best fit using the following equation generates the red curve plotted in the diagram. In all cases, the R^2 associated value with the plot is 0.88.

$$\xi_{(adjusted)} = (45.5/\bar{u}_{NAM}) + 10.9 \tag{5}$$

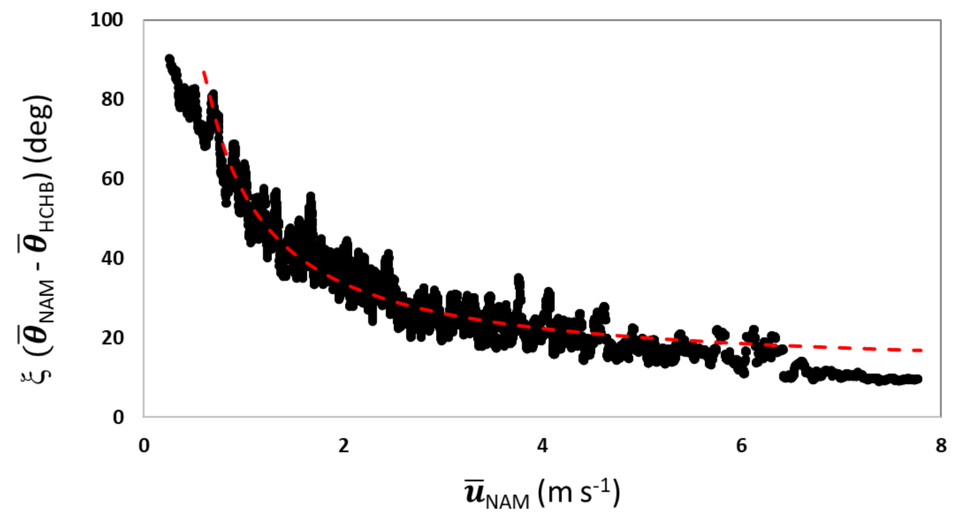

Figure 8: Results of analysis of the uncertainty associated with the difference in wind direction between NAM outputs and HCHB observations against NAM wind speed for the years 2017–2019. The red curve is the result of linear regressions against $1/\bar{u}_{NAM}$. For presentation clarity, every hundredth data point is displayed.

5. Quantifying the Plume Spread Index, σ_θ

The discussion so far has focused on the derivation of the average speed of movement ($\bar{u}$) of a dispersing quantity and the average direction of its movement ($\bar{\theta}$). As required by dispersion computations, estimates of the standard deviation of wind direction fluctuations (σ_θ) must also be derived from the NWP model outputs to describe the direction of the dispersion plume. NWP models, like NAM, are constructed using a Cartesian framework, with velocity presented in terms of two vector components, from the north ($\bar{V}$) and from the west ($\bar{U}$) as already discussed. The

Lagrangian quantities $\bar{u}$ and $\bar{\theta}$ are readily derived from the Cartesian outputs of NAM (as has been done above), but there is no listing provided of the standard deviations associated with the Cartesian components $\bar{U}$ and $\bar{V}$. Dispersion modelers therefore try to derive a best estimate of the plume-relevant Lagrangian quantity σ_θ based on the considered NWP model by interpreting the model outputs. In this section, we are using the HCHB wind observations we are proposing an adjustment of the estimated σ_θ and a quantification of the uncertainty associated with the derivation of σ_θ based on NAM outputs.

In particular, routine NAM model outputs include quantifications of the turbulent kinetic energy (TKE, in units of $m^2\ s^{-2}$), quantified as

$$TKE = (\sigma_u^2 + \sigma_v^2 + \sigma_w^2)/2 \tag{6}$$

The contribution of σ_w^2 is small, amounting to about 7% of the total TKE in slightly unstable conditions (based on the quantifications of the ratios $\sigma_u/u_* = \sigma_v/u_* = 3.5$, and $\sigma_w/u_* = 1.3$, as often quoted — e.g. Garratt. 1992). When transferred to Lagrangian coordinates, this TKE will be approximately equally apportioned between longitudinal and lateral components, so that in the Lagrangian framework

$$\sigma_u = \sigma_v = 0.5\ (0.93 \cdot TKE_{NAM})^{0.5} \tag{7}$$

Since the association of θ with the mean wind speed $\bar{u}$ and the cross-wind quantity σ_v is simply geometric, it follows that as a first order approximation

$$\sigma_\theta = (180/\pi) \cdot atan\ (\sigma_v / \bar{u}) \tag{8}$$

where σ_θ is now expressed in degrees.

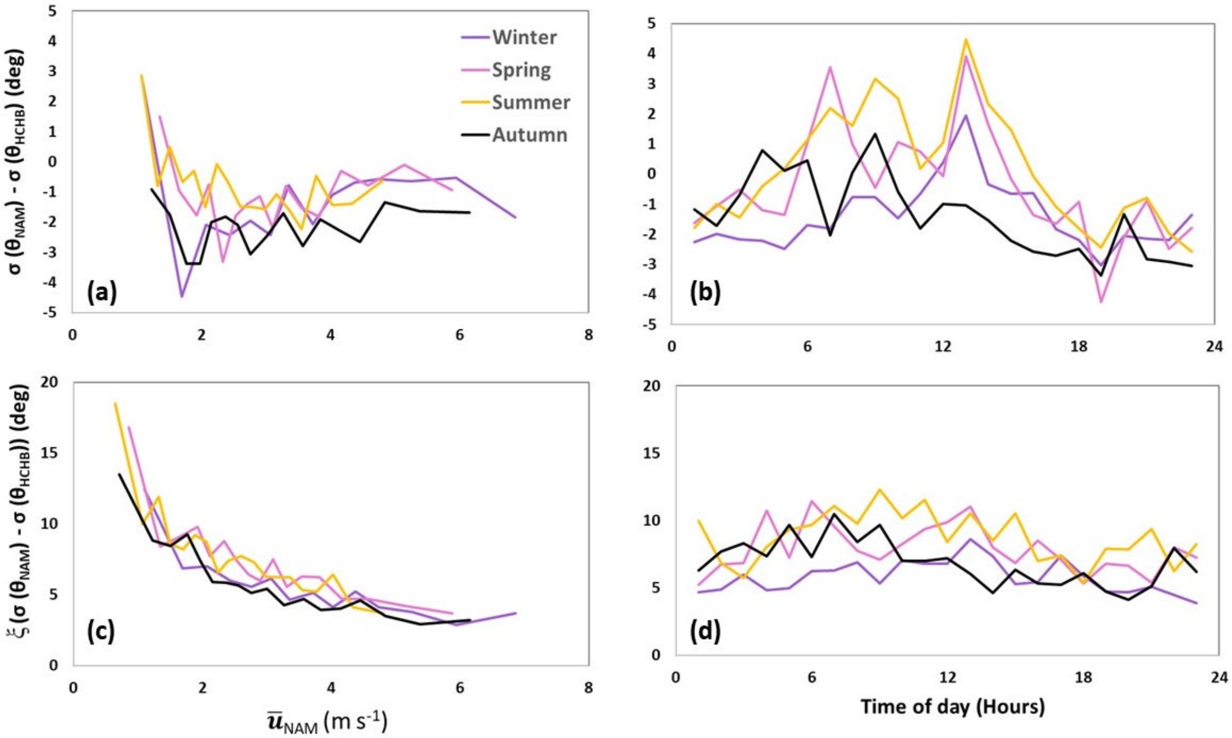

Figure 9: Comparison of the standard deviation of HCHB wind direction ($\sigma_{\theta HCHB}$) and NAM wind direction ($\sigma_{\theta NAM}$) and as a function of NAM wind speed ($\bar{u}_{NAM}$) and as a function of time of day for the four seasons of the year 2018: (a) and (b) the difference between $\sigma_{\theta HCHB}$ and $\sigma_{\theta NAM}$ as a function NAM wind speed and time of day, respectively. (c) and (d) the standard deviation of the difference between $\sigma_{\theta HCHB}$ and $\sigma_{\theta NAM}$ as a function NAM wind speed and time of day, respectively.

Figure 9 compares values of $\sigma_{\theta NAM}$ and $\sigma_{\theta HCHB}$, for the four seasons of 2018. Following the procedures used above, in the context of the average direction of a plume, Figure 9 plots the differences between $\sigma_{\theta NAM}$ and $\sigma_{\theta HCHB}$ and as functions of $\bar{u}_{NAM}$ (in Figure 9a) and time of day (Figure 9b). The lines drawn connect averages (of hundred data points) constructed over sequential groups of observations, after ordering by the abscissa. In Figure 9a there are indications of an increase in the difference between $\sigma_{\theta NAM}$ and $\sigma_{\theta HCHB}$ as wind speed drops below 2 m s^{-1}. This result highlights the fact that the statistical uncertainty related to the differences between $\sigma_{\theta NAM}$ and $\sigma_{\theta HCHB}$ gets higher when NAM wind speed is lower than 2 m s^{-1}. In Figure 9b a slight variation with time of day is evident, but always less than the level of uncertainty indicated in Figure 8d. The averages plotted indicate that a best estimate of σ_θ would be derived from $\sigma_{\theta NAM}$ by the simple expedient of subtracting about 1.5 to 2.5 deg.

The most striking panel of Figure 9 is that which shows how the uncertainty with which σ_θ is computed from NAM outputs varies with wind speed (Figure 9c). As in the case of Figure 8 the data now presented suggest a simple depiction of the uncertainty associated with the derivation of σ_θ such that the level of uncertainty drops according to the reciprocal of the wind speed according to the following equation:

$$\xi\,(\sigma_{\theta\,(adjusted)}) = (10.6/\bar{u}_{NAM}) + 2.1 \qquad (9)$$

in units of degrees.

6. Conclusions

Given that urban-area emergency responders require access to dispersion capabilities for the area of their interest and that on-site observations of the quantities required to initialize such models are usually not available, methods for extracting relevant information from other sources are required. The 12–km scale NAM weather forecasting model, has been used to test the adequacy of its products in the urban dispersion setting. Consideration here has focused on the three input variables common in dispersion calculations: wind speed, wind direction and the standard deviation of the wind direction. Given the complexity flow structure of the urban environment and the scarcity of local wind observations in urban areas, this research provides methods for adjusting NWS model wind outputs based on on-site observations. Adjustments of this kind are necessary to make use of routinely-available weather forecasting predictions to initialize dispersion models over urban areas on which critical decisions for emergency response are based.

Observations of these variables at a centrally-located site in Washington, DC have been used to assess the relevance of NAM outputs and to derive adjustments to them in order to improve their use to initialize dispersion models. In the case of wind speed, the comparisons show that central Washington generally experiences a lower wind speed than NAM predicts, much as expected because the surface roughness of the urban area is greater than that of its surrounding region. There is no consistent variability according to season. The proposed mean adjustment associated with using NAM wind speed predictions tends to be highest in light and high wind conditions (wind speed < 2 m s^{-1}, and wind speed > 5 m s^{-1}), which agrees with other studies showing that meteorological models provide better forecasts for medium range wind conditions (Ngan et al., 2015; Pan et al., 2021; Samalot et al., 2019). The available data analyzed in this study allowed the quantification of the uncertainties associated with such an adjustment that needs to be considered by the modelers.

The wind direction comparison results in a high correlation between NAM predictions and HCHB observations with no consistent dependence on time of day. The results derived when the average difference in wind direction between NAM outputs and HCHB observations are plotted against the NAM wind speed recommended the adjustment of the predicted direction of the plume by -20°. Furthermore, the uncertainty associated with acceptance of this adjustment is large in light winds, decreasing as wind speed increases with no evident variation from season to season. In near-calm conditions, the uncertainty of the adjustment associated with accepting NAM predictions can exceed 60°.

As expected, values of σ_θ derived from NAM outputs underestimate HCHB observations by a few degrees, with no significant trend with either wind speed or time of day. However, the uncertainty associated with imposition of this adjustment changes consistently with wind speed, maximizing in light winds.

The quantified wind forecast errors of NAM model and NWP models in general are related not only to the fact that these models do not include the urban topography, but also to the fact that they are not based on observations within the urban core. Due to the high uncertainty associated with implementing an urban canopy parameterization into fine grid resolution (< 3km) NWP models to explicitly simulate the flows around the surface obstacles of the urban environment (Otte et al., 2004), there is a need to learn how to make best use of the existing local observations to adjust the numerical predictions. The methodology used in reaching these conclusions relies on the availability of a source of representative observations, such as are provided here by a selected station of the DCNet research network. Comparisons of observations from several DCNet stations within the central business district of Washington show that the selected dataset is indeed representative. These results may be taken as an indicative of the circumstances of Washington, D.C., intentionally selected as a research location because of the relative simplicity of the surroundings. Washington, D.C. is on comparatively flat land with a spatial homogeneity that is unusual for a major city. For instance, New York city is certainly different with exceedingly tall buildings and considerable spatial heterogeneity. It was demonstrated that details of building and street orientation can be controlling factors in the movement of pollutants since the air near the surface is affected by the surface obstacles (Grimmond and Oke, 1999). Hicks et al. (2013) analyzed wind observations from six US urban areas in Boston, New York, Philadelphia, Washington, Chicago and New Orleans. They demonstrated that wind speed and velocity component relationships are significantly influenced by local surface inhomogeneities, which require city-dependent consideration.

This study highlights the importance of combining local observations and numerical simulations to resolve the complexity of urban land surfaces. While the present results are encouraging, they confirm expectations and permit quantification of methods for adjustment. However, the extension of these results to other situations would require additional attention.

Acknowledgements

This research was supported by an appointment to the Intelligence Community Postdoctoral Research Fellowship Program at NOAA Air Resources Laboratory Atmospheric Turbulence and Diffusion Division, administered by Oak Ridge Institute for Science and Education through an interagency agreement between the U.S. Department of Energy and the Office of the Director of National Intelligence.

Data Availability

The DCNet observations on the U.S. Department of Commerce Herbert C. Hoover Building for the period 2017-2019 used in this project are included in the published NOAA Technical Memorandum OAR ARL-280: Pendergrass, W., Lichiheb, N., White, R., Hicks, B., Myles, L., 2020. ARL Tech Memo: HighResolution Meteorological Monitoring over the National Capital Region: Data from the DCNet Network at the US Department of Commerce Herbert C. Hoover Building Station. TM-280. All the DCNet data are stored and archived at the NOAA ARL, ATDD in Oak Ridge, Tennessee. These data are available on request.

The operational 12 km NAM forecasts for the period 2017-2019 used in this project can be found on the NCEP ftp server (ftp://ftpprd.ncep.noaa.gov/pub/data/nccf/com/nam/prod/nam.20211107/) or on the National Center for Atmospheric Research (NCAR) website (https://rda.ucar.edu/datasets/ds609.0/#!docs).

Reference

Arnfield, A. J., 2003: Two decades of urban climate research: a review of turbulence, exchanges of energy and water, and the urban heat island. *Int. J. Climatol*., **23**,1–26, https://doi.org/10.1002/joc.859.

Baklanov, A., Grimmond, C.S.B., Carlson, D., Terblanche, D., Tang, X., Bouchet, V., Lee, B., Langendijk, G., Kolli, R.K., Hovsepyan, A., 2018: From urban meteorology, climate and environment research to integrated city services. *Urban Clim*., **23**, 330-341, https://doi.org/10.1016/j.uclim.2017.05.004.

Black, T., 1994: The new NMC mesoscale Eta model: Description and forecast examples. *Wea. Forecasting*,**9**,265–278,https://doi.org/10.1175/1520 0434(1994)009%3C0265:TNNMEM%3E2.0.CO;2.

Britter, R. E. and Hanna, S.R., 2003: Flow and dispersion in urban areas. *Annu. Rev. Fluid Mech*., **35**, 469-496, 10.1146/annurev.fluid.35.101101.161147.

Dabberdt, W. F., Hales, J., Zubrick, S., Crook, A., Krajewski, W., Doran, J.C., Mueller, C., King, C., Keener, R.N., Bornstein,R., Rodenhuis, D., Kocin,P., Rossetti, M.A., Sharrocks, F., Stanley, E.M., 2000: Forecast issues in the urban zone: Report of the10th prospectus development team of the U.S. Weather Research Program. Bull. *Amer. Meteor. Soc*., **81**, 2047–2064, https://ui.adsabs.harvard.edu/link_gateway/2000BAMS...81.2047D/doi:10.1175/1520-0477(2000)081%3C2047:FIITUZ%3E2.3.CO;2.

Draxler, R.R., 1987a: One year of tracer dispersion measurements over Washington, D.C. *Atmos. Environ*, **21**, 69-77, https://doi.org/10.1016/0004-6981(87)90272-1.

Draxler, 1987b: Accuracy of various diffusion and stability schemes over Washington, DC. *Atmos. Environ*., **21**, 491–499, https://doi.org/10.1016/0004-6981(87)90032-1.

Garratt, J. R., 1992: The Atmospheric Boundary Layer. University Press, 316 pp.

Grimmond, C. S. B., Oke, T. R., 1999. Aerodynamic Properties of Urban Areas Derived from Analysis of Surface Form. *J. App. Meteor.*, ***38***, 1262-1292. https://doi.org/10.1175/1520-0450(1999)038<1262:APOUAD>2.0.CO;2 .

Hand, L.M., Shepherd, J.M., 2009: An investigation of warm-season spatial rainfall variability in Oklahoma City: possible linkages to urbanization and prevailing wind. *J Appl Meteorol Climatol*, **48**, 251-269, .

Haupt, S. E., Hanna, S., Askelson, M., Shepherd, M., Fragomeni, M. A., Debbage, N., & Johnson, B., 2019. 100 Years of Progress in Applied Meteorology. Part II: Applications that Address Growing Populations, *Meteorol.Monogr.*, **59**, 23.1-23.40, https://doi.org/10.1175/AMSMONOGRAPHS-D-18-0007.1 .

Hicks, B. B., W. R. Pendergrass, C. A. Vogel, and R. S. Artz, 2014: On the Drag and Heat of Washington, D.C., and New York City. *J. Appl. Meteor. Climatol.*, **53**, 1454–1470, https://doi.org/10.1175/JAMC-D-13-0154.1 .

Hicks, B.B., Novakovskaia, E., Dobosy, R.J., III, W.R.P., Callahan, W.J., 2013. Temporal and Spatial Aspects of Velocity Variance in the Urban Surface Roughness Layer. *J. Appl. Meteor. Climatol*., **52**, 668-681.

Hicks, B. B., Callahan, W. J., Pendergrass III, W. R., Dobosy, R. J. and Novakovskaia, E. 2012: Urban turbulence in space and time. *J. Appl. Meteor. Climatol*., **51**, 205–218, https://doi.org/10.1175/JAMC-D-11-015.1 .

Hicks, B.B., Callahan, W.J. & Hoekzema, M.A., 2010: On the Heat Islands of Washington, DC, and New York City, NY. *Boundary-Layer Meteorol* **135,** 291–300, http://dx.doi.org/10.1007/s10546-010-9468-1 .

Hicks, B.B., 2005: Urban dispersion for the 21st century. WIT Transactions on The Built Environment**, 82**, 555-566.

Kanda, M., 2007: Progress in Urban Meteorology: A Review. *Journal of the Meteorological Society of Japan. Ser. II,* **85B**, 363-383.

Kelly, F.J., Fussell, J.C., 2015: Air pollution and public health: emerging hazards and improved understanding of risk. *Environ. Geochem. Hlth*., **37,** 631-649, https://doi.org/10.1007/s10653-015-9720-1 .

Leeson, G.W., 2018: The Growth, Ageing and Urbanisation of our World. *Population Ageing,* **11,** 107–115.

Martilli, A., 2002. Numerical Study of Urban Impact on Boundary Layer Structure: Sensitivity to Wind Speed, Urban Morphology, and Rural Soil Moisture, *J. App. Meteor.*, ***41***, 1247-1266. https://doi.org/10.1175/1520-0450(2002)041<1247:NSOUIO>2.0.CO;2.

McMillen RT, 1988: An eddy-correlation technique with extended applicability to non-simple terrain. *Boundary Layer Meteorol*, **43**, 231-245.

NCAR, 2021: NCEP North American Mesoscale (NAM) 12 km Analysis. Available as doi:10.5065/G4RC-1N91.

Ngan, F.; Cohen, M.; Luke, W.; Ren, X.; Draxler, R., **2015**: Meteorological Modeling Using the WRF-ARW Model for Grand Bay Intensive Studies of Atmospheric Mercury. *Atmosphere*, ***6***, 209-233, https://doi.org/10.3390/atmos6030209.

Oke, T. R., 1987: BoundaryLayer Climates. 2nd ed., Methuen, 435 pp.

Otte, T. L., Lacser, A., Dupont, S., Ching, J. K. S., 2004. Implementation of an Urban Canopy Parameterization in a Mesoscale Meteorological Model, *J. App. Meteor.*, ***43***, 1648-1665. https://doi.org/10.1175/JAM2164.1 .

Pan, L.; Liu, Y.; Roux, G.; Cheng, W.; Liu, Y.; Hu, J.; Jin, S.; Feng, S.; Du, J.; Peng, L., 2021: Seasonal variation of the surface wind forecast performance of the high-resolution WRF-RTFDDA system over China. *Atmos. Res.*, ***259***, 105673, https://doi.org/10.1016/j.atmosres.2021.105673 .

Pataki DE, Xu T, Luo YQ, Ehleringer JR, 2007: Inferring biogenic and anthropogenic carbon dioxide sources across an urban to rural gradient. *Oecologia*, **152**, 307-322, https://doi.org/10.1007/s00442-006-0656-0 .

Pendergrass, W., Lichiheb, N., White, R., Hicks, B., Myles, L., 2020: ARL Tech Memo: High-Resolution Meteorological Monitoring over the National Capital Region: Data from the DCNet Network at the US Department of Commerce Herbert C. Hoover Building Station. TM-280, https://doi.org/10.25923/ x74e-3k77.

Roth, M., 2000: Review of atmospheric turbulence over cities. *Q. J. R. Meteorol. Soc.*, **126**, 941-990, https://doi.org/10.1002/qj.49712656409.

Samalot, A., Astitha, M., Yang, J., Galanis, G., 2019: Combined Kalman Filter and Universal Kriging to Improve Storm Wind Speed Predictions for the Northeastern United States. *WAF* **34**, 587-601, https://doi.org/10.1175/WAF-D-18-0068.1 .

Seaman, N. L., 2000: Meteorological modeling for air quality assessments. *Atmos. Environ.*, **34**, 2231–2259, https://doi.org/10.1016/S1352-2310(99)00466-5 .

Shepherd, J., M., 2006: Evidence of urban-induced precipitation variability in arid climate regimes. *J Arid Environ*, **67**, 607-628, https://doi.org/10.1016/j.jaridenv.2006.03.022 .

Stewart, I. D., and T. R. Oke, 2012: Local climate zones for urban temperature studies. *Bull. Amer. Meteor. Soc.,* **93**, 1879–1900, https://doi.org/10.1175/BAMS-D-11-00019.1 .

United Nations, 2019: World Urbanization Prospects, the 2018 revision. Department of Economic and Social Affairs. ST/ESA/SER.A/420, 103pp.

Yang, L., J. A. Smith, D. B.Wright, M. L. Baeck, G. Villarini, F. Tian, and H. Hu, 2013: Urbanization and climate change: An examination of nonstationarities in urban flooding. J. *Hydrometeor.*, **14,** 1791–1809.